

# On the design of end tabs for quasi-static and fatigue testing of fibre-reinforced composites

I. De Baere, W. Van Paepegem and J. Degrieck

Department of Mechanical Construction and Production, Faculty of Engineering, Ghent University. Sint-Pietersnieuwstraat 41, B-9000 Gent, Belgium.

E-mail: Ives.DeBaere@UGent.be

## Abstract

The use of end tabs is often necessary when performing quasi-static uni-axial tests on fibre-reinforced composites. However, finding a suitable combination of material and geometry for these end tabs in order to have acceptable and reproducible results may be a problem. In this paper four different geometries and four different materials of the tabs are numerically examined for the tensile testing of a carbon fabric reinforced polyphenylene sulphide. First, it is assessed if a simplified finite element model of a tensile grip is acceptable. Then, this simplified model is used to examine the proposed setups. It may be concluded that, for the given material, short straight end tabs with a  $[(0^\circ, 90^\circ)]_{4s}$  lay-up should be used and the specimen should be mounted in such a way that the end tabs are completely between the grips.

## 1. Introduction

When performing quasi-static tests on fibre-reinforced materials, the use of end tabs is often necessary to prevent clamp failure. The ASTM D3039/D3039M *Standard Test Method for Tensile Properties of Polymer Matrix Composite Materials*, states that tabs are not required, but the need to use tabs should be determined by the experiments themselves. If acceptable failure modes occur with reasonable frequency, then there is no need to change the gripping method. However, if grips are required, the standard gives some recommendations considering the tab dimensions. Summarized, a continuous glass fibre-reinforced polymer with  $[+45^\circ/-45^\circ]_{ns}$  laminate configuration should be used, the length should be about 50 mm and the bevel angle should be 7 or 90 degrees, depending on the stacking sequence of the test material. When gripping the specimen, the grips should overhang the bevelled portion of the tab by approximately 10 to 15 mm. For the tab material, the same material as the one being tested or aluminium can also give good results.

It is also stated that ‘sufficient’ lateral pressure should be used to avoid slipping.

The ISO 527-1 *International standard for the determination of tensile properties* gives similar recommendations: the tabs should have a length larger than or equal to 50 mm, the angle should be 90 degrees and the jaws should overhang the tabbed section. For the material, a cross-ply glass fibre-reinforced polymer with the fibres at  $\pm 45^\circ$  to the tensile direction is suggested.

When performing uni-axial fatigue tests, clamp failure is even more likely to occur. The ASTM D3479/D3479M *Standard Test Method for Tension-Tension Fatigue of Polymer Matrix Composite Materials* states that end tabs should always be used, using the same geometry recommendations as in the ASTM D3039/D3039M Standard.

Both standards suggest a tab length of at least 50 mm and the grips should overhang the end of the tab by about 10 mm. However, in some cases, this may cause problems. Figure 1 shows two standard INSTRON™ grips for tensile testing. The jaws are 57 mm long, so if tabs of 50 mm are used, only 7 mm is left, of which only 4 mm is serrated and therefore actually grips the specimen. So problems may occur in the following cases:

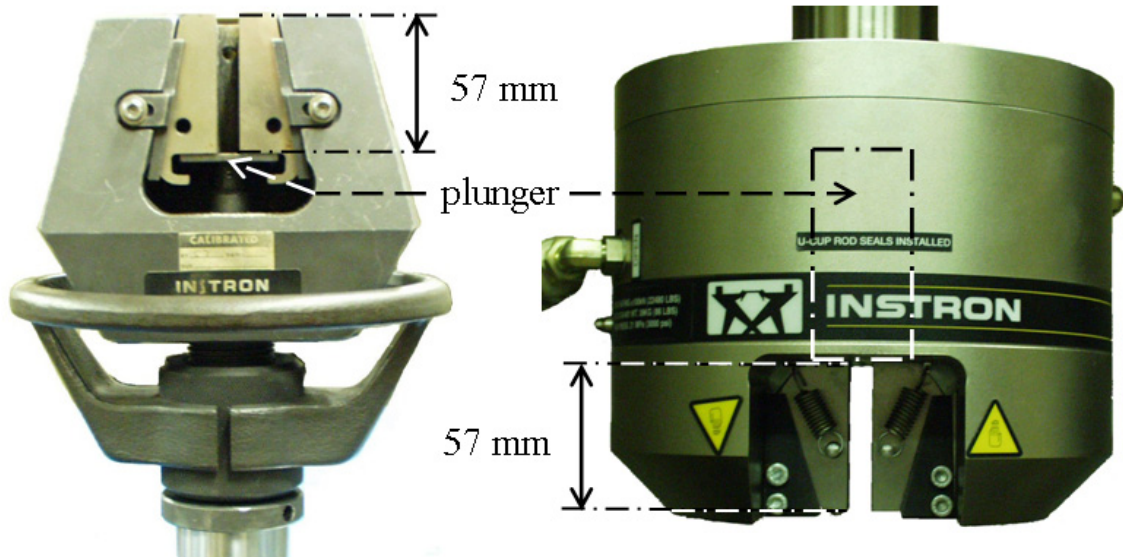


Figure 1 The Instron™ mechanical grips (left) and hydraulic grips (right).

(i) some composites or plastics are difficult to bond, because of their chemical inertness, resulting in low ultimate shear stress of the adhesive. By increasing the surface area of the tabs, the fracture load of the specimen can be reached before ultimate shear stress of the adhesive is reached. For example, the used material for the experiments in this article is a carbon fibre-reinforced Polyphenylene Sulphide (PPS) which has an ultimate stress of about 770 MPa. Since PPS is not easily bonded, the ultimate shear strength of the adhesive is about 15 MPa or less. By writing the equilibrium in the adhesive layer, the required length of the tabs can be derived:

$$\sigma_{ult}^{specimen} \cdot w^{specimen} \cdot t^{specimen} = 2 \cdot \tau_{ult}^{glue} \cdot w^{tab} \cdot l^{tab} \quad (1)$$

The width of the specimen ( $w^{specimen}$ ) is equal to the width of the tab ( $w^{tab}$ ), a typical thickness of this composite specimen is 2.4 mm. If all these values are implemented in the equation, the tab length is equal to 61.6 mm, which means that the tabbed section is outside the jaws.

(ii) another problem occurs when the specimen requires extra space at the ends for special fixtures or sensors. For instance, if the longitudinal strain is measured with an optical fibre sensor [3, 4, 5, 6], this fibre comes out of the specimen at the end (Figure 2). Since this fibre breaks off very easily, it requires some space so that it can be bent with a relatively large radius. As such, the tabs will be outside the jaws.



Figure 2 An optical fibre at the end of a test specimen. To protect the optical fibre during production and handling of the specimen, a kapton coating was added.

Another type of in-situ monitoring for composites is the use of the carbon fibre-reinforcement for electrical resistance measurement. In some cases the contact electrodes are placed outside the tabs in the strain free area, as described in [7, 8, 9, 10, 11]. For example, the setup used in [11] is illustrated in Figure 3, where the gripping of such a specimen with standard clamps is shown. The end of the specimen may not touch the clamps, because the specimen should be electrically isolated from the tensile machine. It is clear that more space should be available. With these clamps, only 35 mm of the available 50 mm of tab-length is gripped.

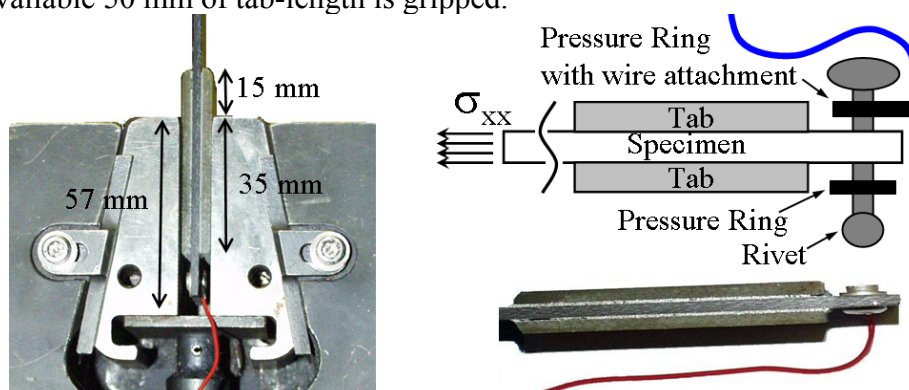


Figure 3 Contact electrode used in [11], which illustrates the gripping problem.

As may be concluded from the paragraphs above, the ASTM and ISO standards can only give recommendations. The ASTM D3039/D3039M even mentions that ‘*Design of mechanical test coupons remains to a large extent an art rather than a science*’. The goal of this article is to examine a few possible tab geometries, presented in Figure 4, by using finite element modelling. The effect of the tabs being completely inside or partly outside the grips is examined, as well as the effect of the magnitude of the grip pressure. The latter cannot be controlled with mechanical clamps (Figure 1 on the left) but can be adjusted when using hydraulic clamps (Figure 1 on the right).

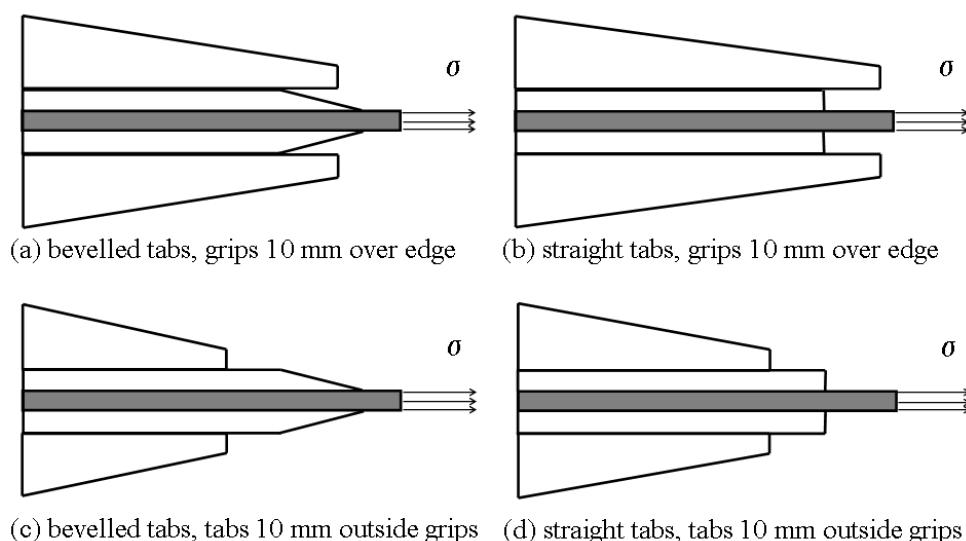


Figure 4 Different tab and clamping setups, discussed in this paper.

First, the used material for the experiments is discussed. Then, the modelling of the setup is discussed. This is followed by the numerical simulations. Finally, some conclusions are drawn and a suggestion is made for a possible geometry.

## 2. Materials and Methods

### 2.1. Composite Material

The material under study was a carbon fibre-reinforced polyphenylene sulphide (PPS), called CETEX™. This material was supplied by Ten Cate. The fibre type is the carbon fibre T300J 3K and the weaving pattern is a 5-harness satin weave with a mass per surface unit of 286 g/m<sup>2</sup>. The 5-harness satin weave is a fabric with high strength in both directions and excellent bending properties.

The carbon PPS plates were hot pressed, only one stacking sequence was used for this study, namely a [(0°,90°)]<sub>4s</sub> where (0°,90°) represents one layer of fabric.

The in-plane elastic properties of the individual carbon PPS lamina were determined by the dynamic modulus identification method as described in [1] and are listed in Table 1.

The very low value of the Poisson's ratio must be noted.

Table 1 In-plane elastic properties of the individual carbon/PPS lamina (dynamic modulus identification method).

$E_{11}$	56.0	GPa
$E_{22}$	57.0	GPa
$\nu_{12}$	0.033	-
$G_{12}$	4.175	GPa

The tensile strength properties were supplied by Ten Cate Advanced Composites and are listed in Table 2.

Table 2 Tensile strength properties of the individual carbon/PPS lamina (Mechanical testing at TUDelft).

$X_T$	767.0	MPa
$\epsilon_{11}^{ult}$	0.011	-
$Y_T$	754.0	MPa

$\epsilon_{22}^{ult}$	0.013	-
$S_T$	110.0	MPa

The test coupons were sawn with a water-cooled diamond saw, the dimensions are given in Figure 5 for the straight end tabs.

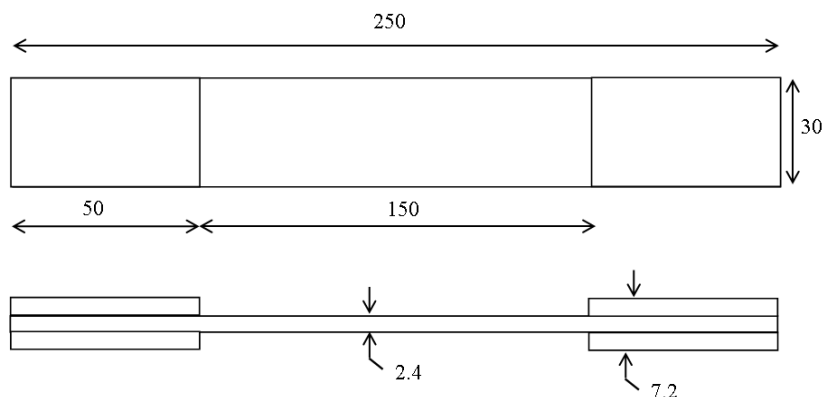


Figure 5 Dimensions of the tensile coupon used for the experiments.

## 2.2. Equipment

All tensile tests were performed on a servo hydraulic INSTRON 8801 tensile testing machine, equipped with hydraulic clamps, a FastTrack 8800 digital controller and a load cell of  $\pm 100$  kN. The quasi-static tests were displacement-controlled with a speed of 2 mm/min.

For the registration of the tensile data, a combination of a National Instruments DAQpad 6052E for fireWire, IEEE 1394 and the SCB-68 pin shielded connector were used. The load, displacement and strain, given by the FastTrack controller were sampled on the same time basis.

## 3. Finite element modelling

### 3.1. Introduction

In [2], the authors have derived a formula for a setup illustrated in Figure 6 that describes the interaction between the load  $F$  on the specimen, the force  $R_A$  of the plunger (see Figure 1) represented by part A and the contact force  $P$  on the specimen.

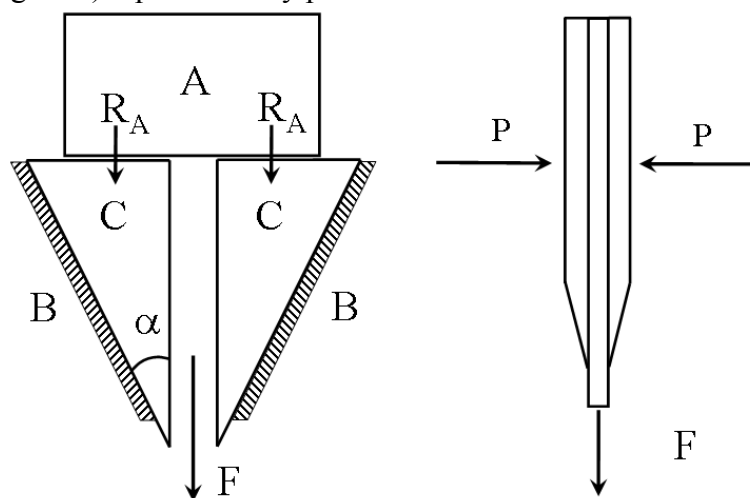


Figure 6 Symbolic representation of the gripping principle of a clamp.

The following equation was derived, with  $\mu_{ij}$  the coefficient of friction between parts  $i$  and  $j$  ( $i,j=A,B,C$ ):

$$P = \frac{F \cos \alpha - \mu_{BC} \sin \alpha}{2 \sin \alpha + \mu_{BC} \cos \alpha} + R_A \frac{(1 - \mu_{AC} \mu_{BC}) \cos \alpha - (\mu_{BC} - \mu_{AC}) \sin \alpha}{\sin \alpha + \mu_{BC} \cos \alpha} \quad (2)$$

For both grips displayed in Figure 1, the angle  $\alpha$  is equal to 10 degrees.

In the next paragraph, this formula is verified by means of finite element modelling of the total gripping mechanism. This has been done in ABAQUS™/Standard v6.6-2.

### 3.2. Modelling of the entire clamp

Figure 7 illustrates the simulated parts in the finite element model. Because of symmetry, only half of the clamp is modelled, which reduces calculation time. The corresponding symmetry boundary conditions have been imposed on the specimen. To further reduce computation time, a rigid body constraint is placed on part of the cylinder, only the area where the cylinder makes contact with the grip is left deformable. Furthermore, a part that models the plunger is added, also with a rigid body constraint to reduce calculation time. The reference point of this part is given a certain downward displacement. It must be noted that this part could be omitted and replaced by a downward force on top of the grip. This force would be equal to  $R_A$  in the deduction in the previous paragraphs. However, when doing so, the simulation required a lot of calculation time and often did not converge to a solution. Therefore, this model was used and a corresponding value of  $R_A$  was derived from the reaction force in the reference point of the plunger.

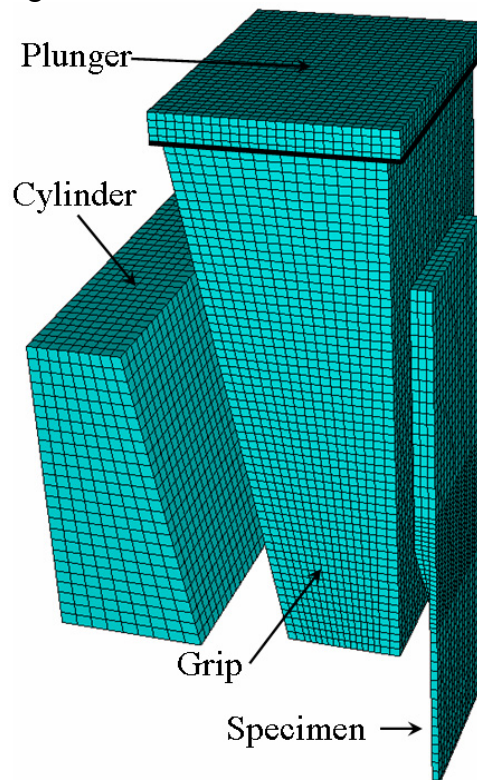


Figure 7 The simulated clamp in the finite element model.

Two time steps were implemented: in the first, the wedge was given a downward motion of 0.75 mm, simulating the tightening of the grips; in the second, the bottom of the specimen was pulled down over 1 mm, simulating a tensile test.

Contact conditions were imposed between the surfaces of the specimen and the grip, the grip and the cylinder and the grip and the wedge. Since the grip first follows the movement of the wedge and then the movement of the specimen, the slave surfaces of all contact conditions mentioned, were placed on the grips. Between specimen and grip, the tangential behaviour ‘rough’ was implemented, which means that no slip occurs once nodes make contact. For the other contact conditions, the ‘lagrange’ condition was used, which means that the tangential force is  $\mu$  times the normal force,  $\mu$  being the friction coefficient. The same friction coefficient was used for both conditions.

The grip was meshed with a C3D8R element, a linear brick element with reduced integration, whereas all other parts were meshed with C3D20R, a quadratic brick element with reduced integration. The C3D8R of the grip is required instead of the C3D20R, since the slave surfaces require midface nodes and the C3D20R do not have one.

For the grip, the wedge and the cylinder, steel was implemented with a Young’s modulus of 210000 MPa and a Poisson’s ratio of 0.3. The specimen was a composite material with the following elastic properties (Table 3).

Table 3 The implemented engineering constants in the finite-element model for the specimen.

$E_{11}$ [MPa]	56000	$\nu_{12}$ [-]	0.033	$G_{12}$ [MPa]	4175
$E_{22}$ [MPa]	57000	$\nu_{13}$ [-]	0.3	$G_{13}$ [MPa]	4175
$E_{33}$ [MPa]	9000	$\nu_{23}$ [-]	0.3	$G_{23}$ [MPa]	4175

Two simulations were performed, one with  $\mu$  equal to 0.1 and one with  $\mu$  equal to 0, which means no friction occurred. A value for  $R_A$  is derived from the reaction force of a reference point on top of the wedge and a value for  $F$  is calculated from the longitudinal stress in the specimen. With both values, an average contact pressure  $p$  can be calculated using Equation 2 and the following equation, with  $A_{tab}$  the surface of the contact area between tab and specimen:

$$p = \frac{P}{A_{tab}} \quad (3)$$

In Equation 2, all friction coefficients  $\mu_{ij}$  were taken equal to  $\mu$  used for both simulations.

For comparison, an average contact pressure for the ABAQUS™ simulation is calculated by integrating the local contact pressure over the surface, yielding a resultant force, and dividing this resultant force by the surface of the tab  $A_{tab}$ .

An overview of both simulations is given in Table 4. Each simulation took about 33 hours of calculation time.

Table 4 Results of both the ABAQUS™ simulation and the prediction with the derived model (Equation 2 and 3).

Friction coefficient $\mu$	[-]	0.0	0.1
Force $F$	[kN]	17.89	16.43
Force $R_A$	[kN]	3.78	18.09
Averaged $p$ (ABAQUS™)	[MPa]	<b>67.33</b>	<b>66.97</b>
Predicted $p$ (Equation 2 & 3)	[MPa]	<b>68.26</b>	<b>68.45</b>

It may be concluded that the theoretical model from [2] predicts the actual value very well. Finally, Figure 8 illustrates the actual contact stress distribution for the simulation

with a friction coefficient equal to 0 together with the prediction mentioned above. The simulations with  $\mu$  equal to 0.1 yielded a similar contact stress distribution.

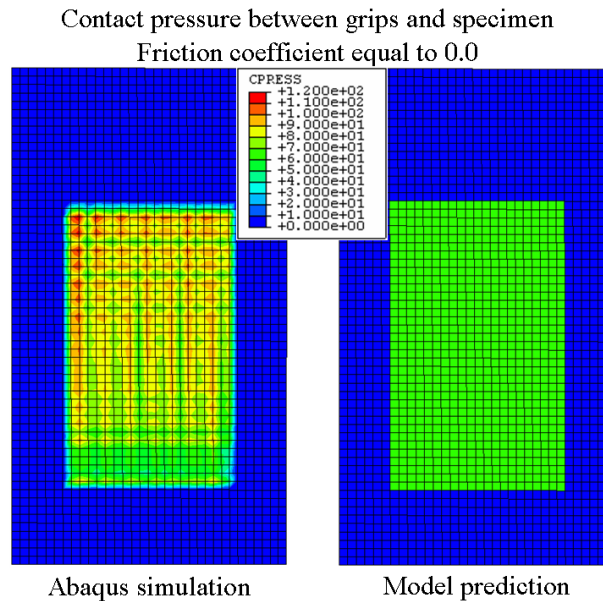


Figure 8 Illustration of the contact-stress distribution, calculated with  $\mu = 0.0$  for both the ABAQUS™ simulation and the prediction with the derived model.

It may be noted that in the ABAQUS™ simulation, the contact pressure is not evenly distributed, but seems to have stress concentrations. This, however, is a result of the combination of the used C3D8R elements for the grip and the ‘Rough’ contact condition. The ‘Rough’ contact condition was implemented because it is the most accurate description of the real conditions, where the grips have a serrated surface and once the teeth penetrate the specimen surface, no slip occurs. Figure 9 shows the contact pressure between the grip and the cylinder (see Figure 7) where the contact condition ‘Rough’ was replaced by a ‘Lagrange’ law with a friction coefficient of 0.1. It can be seen that the pressure evolves more fluently and is not ‘spiky’ as is the case in Figure 8.

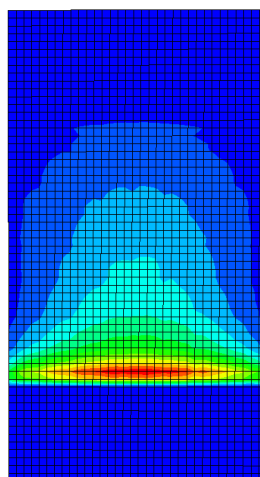


Figure 9 Distribution of the contact stress between the grip and the cylinder. The contact condition was ‘Lagrange’ with  $\mu$  equal to 0.1.

Since Equation 2 is accurate enough to predict the contact pressure, there is no need to model the entire clamp to investigate the different setups proposed in Figure 4. For a

given load in the specimen and a given force from the plunger, the contact pressure can be estimated by Equations 2 and 3. Therefore, a simplified model can be used.

For this simplified model, first a choice must be made concerning the dimensions of the tabs. The first possibility is to have equal tab length for all the setups in Figure 4. As a result, it would be very easy to compare the stress distributions along the tabbed section for the different geometries, for instance the location of possible stress concentrations. However, since the surface area of the gripped zone varies (tabs inside the grips or 10 mm outside the grips) this would result in different contact pressures for a given grip force  $P$ , given by Equation 2 and therefore, stresses resulting from different load cases are compared.

The second possibility is to have an equal contact pressure for all the setups. This gives more meaning to the comparison of stress distributions and stress concentrations, since they are the result of the same original loads. Of course, this results in different tab lengths, depending on the gripping setup. The authors have chosen for the second option because the comparison of the stress distributions is more valid in this case.

According to the standards described above, the clamped section was always chosen 50 mm. Depending on the gripping setup (Figure 4) this leads to simulated tab lengths of 60 mm for setup a, 50 mm for setup b, 70 mm for setup c and 60 mm for setup d. Since the thickness of the tabs is 2.4 mm, this results in a bevelled angle of  $13.5^\circ$  for the chamfered tabs in setups b and c.

The final configurations are depicted in Figure 10:

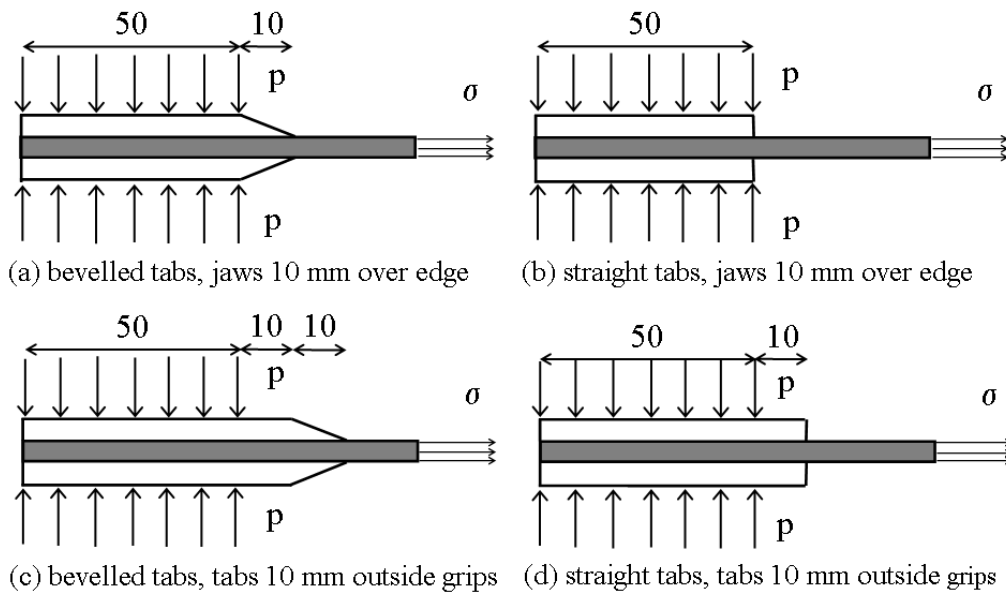


Figure 10 Different gripping setups, simplified model.

### 3.3. Finite element simulation of a simplified model

The finite element models of the four setups are similar to each other; the specimen for setup c is discussed. Figure 11 shows the model of this setup, both mesh and boundary conditions are illustrated.

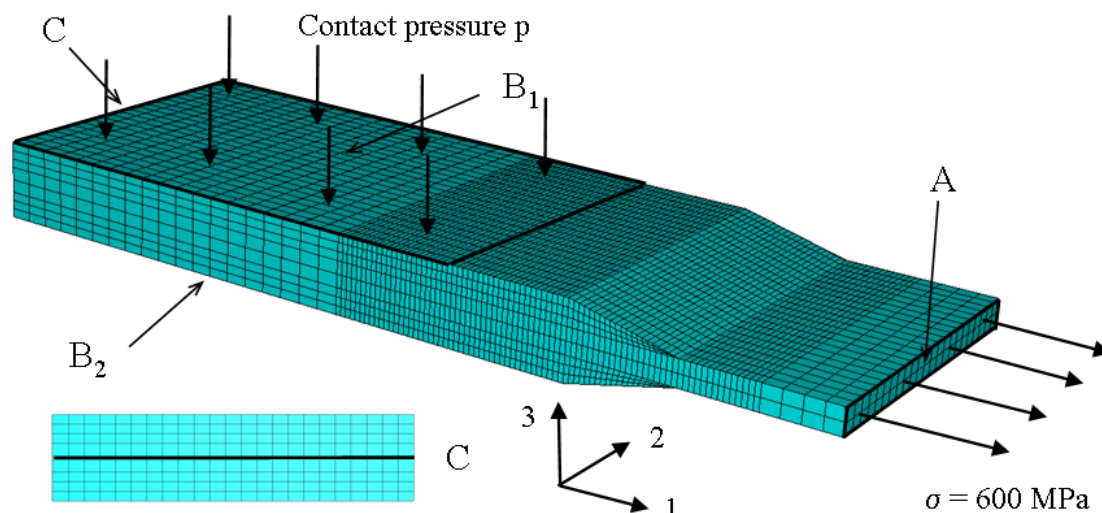


Figure 11 Illustration of the model for specimen type c.

The specimen is meshed using C3D20R elements using a global element size of 2 mm. Where stress concentrations were expected, the element size was reduced to 0.5 mm. The thickness of the specimen was 2.4 mm, which is also the thickness of the tabs, as has already been mentioned. The material properties for the composite specimen are given in Table 3.

For the boundary conditions, the displacement along the 1 and 2 axis was inhibited for planes  $B_1$  (on top) and  $B_2$  (at the bottom), simulating the ‘rough’ boundary condition from the previous paragraph. Since contraction of the specimen is possible in the 3-direction due to the Poisson effect, the movement along the 3-axis was allowed for both planes. In order to prevent movement of the entire sample along the 3 axis, the central line of plane C (at the back) was fixed.

Two time steps were modelled. In the first, the contact pressure  $p$ , calculated with Equation 3, was imposed. In the second, a tensile stress of 600 MPa was applied on surface A. The exact value of the stress does not matter, since the stress concentration factors will be compared. The authors have chosen this value, since most of the experiments ended at about 600 MPa. The low fracture stress compared to the one given in Table 2 is due to preliminary failure inside or under the edge of the tabs. This would mean that there is a stress concentration factor of about 1.25.

For the contact pressure, two series of calculations were done. The first represents the mechanical clamps in Figure 1, which corresponds with  $R_A$  equal to zero and the contact pressure  $p$  equal to 51.19 MPa. The second corresponds with the hydraulic clamps. For these clamps, INSTRON suggests a gripping pressure that is correlated with the applied load, because in a fatigue experiment, the grips should be pre-stressed so that the grips themselves are not fatigued. For the given load level of 600 MPa tension, INSTRON suggests a gripping pressure of 68 bar. As a result,  $R_A$  becomes about 10 kN and  $p$  is equal to 76.52 MPa.

Concerning the tab material, the following setups were tested.

- (i) Carbon fabric reinforced PPS, using a  $[(+45^\circ, -45^\circ)]_{4s}$  setup, which is suggested by the standards. The mechanical properties are the same as in Table 3.
- (ii) Glass fabric reinforced epoxy, using a  $[(+45^\circ, -45^\circ)]_{4s}$  setup, which is also suggested by the standards. The mechanical properties are given in Table 5

Table 5 The implemented engineering constants in the finite-element model for the glass-epoxy tabs.

$E_{11}$ [MPa]	24000	$\nu_{12}$ [-]	0.153	$G_{12}$ [MPa]	4830
$E_{22}$ [MPa]	24000	$\nu_{13}$ [-]	0.153	$G_{13}$ [MPa]	4830
$E_{33}$ [MPa]	10000	$\nu_{23}$ [-]	0.153	$G_{23}$ [MPa]	4830

(iii) Aluminium tabs, mentioned in the standards. The stiffness is equal to 70000 MPa and Poisson's ratio is 0.3.

(iv) Carbon fabric reinforced PPS, using a  $[(0^\circ, 90^\circ)]_{4s}$  setup, with the same mechanical properties as the sample. In this setup, there is no sudden change in the elastic properties between the specimen and the tab in the xyz coordinate system (x being the tension direction and z the through-thickness direction). The authors expect that this would result in lower stress concentrations.

Finally, the stress concentrations may also be the result of the used geometry of the specimen instead of the orthotropic nature of the composite and the combination of different materials. For example, it is well known that a sudden change in cross section of a structure causes stress concentrations. To assess if this also occurs here, the entire setup has also been modelled in isotropic material, in this case steel, with a stiffness of 210000 MPa and Poisson's ratio 0.3.

A preliminary examination of the results yielded that the stress concentrations were the highest at the surface of the specimen. Therefore, the longitudinal stress  $\sigma_{xx}$  was plotted along a path central on the surface of the specimen. A typical result of this evolution is given in Figure 12 for the setup with the straight-end glass epoxy tabs, mounted inside the grips. Both the simulation with  $R_A = 0$  and  $R_A = 10$  kN are depicted.

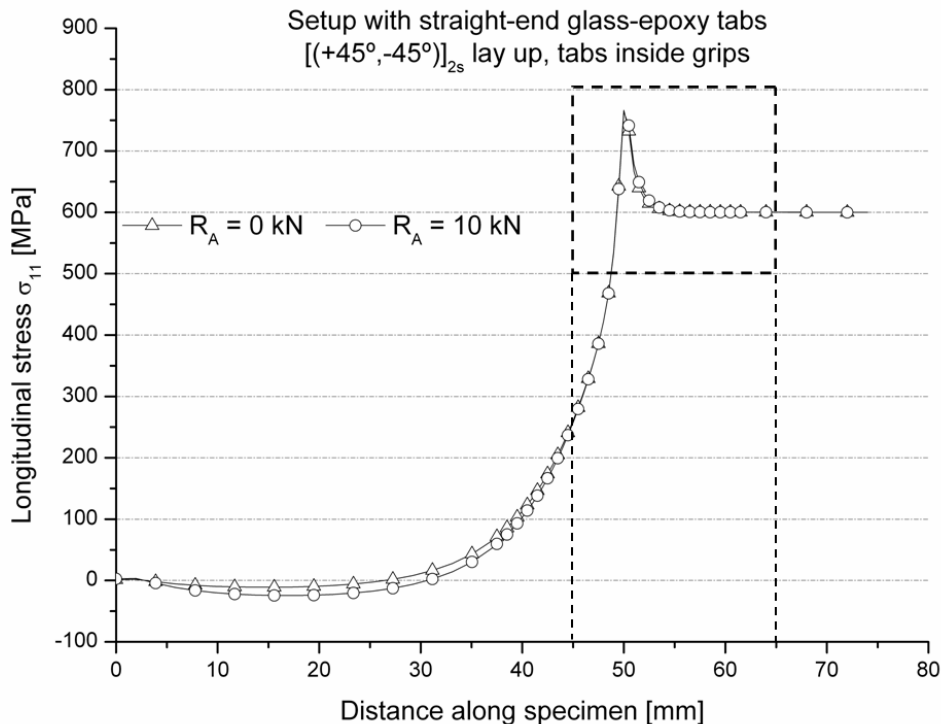


Figure 12 Evolution of the longitudinal stress along the surface of the specimen for setup b.

It may be remarked that the value of  $R_A$  does not seem to have a very large influence, although the contact pressure is fifty percent higher for  $R_A$  equal to 10 kN. Only underneath the tab, it seems to have some influence. Furthermore, it was noted that all of the graphs of the different setups showed an evolution similar to the one depicted. Since we are only interested in the zone around the peak stress, only the evolution inside the indicated rectangle in Figure 12 is considered. For an easier comparison of the

different setups, the stress concentration factor is plotted instead of the absolute stress value, since the latter depends on the load in the specimen. This factor SFC is given by:

$$SFC = \frac{\sigma_{11}}{600MPa} \quad (4)$$

#### 4. Discussion of the simplified model simulations

Figure 13 till Figure 16 give the evolution of SFC for the different setups. It may be remarked that the value of  $R_A$  does not seem to have any influence on the values of the stress concentration factor, although the contact pressure is fifty percent higher for  $R_A$  equal to 10 kN. Only in Figure 14, a small difference between the curves of two corresponding setups may be distinguished. The position of the highest stress is always exactly behind the end of the tab. All stress concentration factors are summarised in Table 6 for the calculations with  $R_A = 0$  and in Table 7 for  $R_A = 10$  kN.

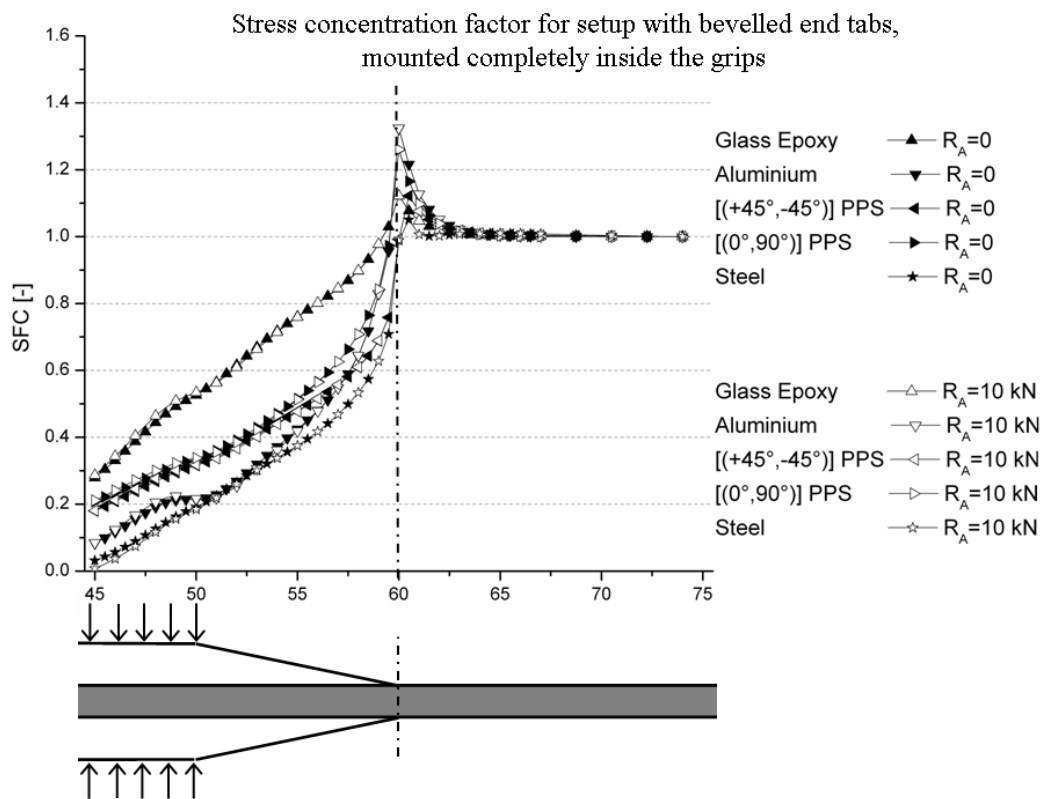


Figure 13 Detail of the evolution of the stress concentration factor along the surface of the specimen for geometry a.

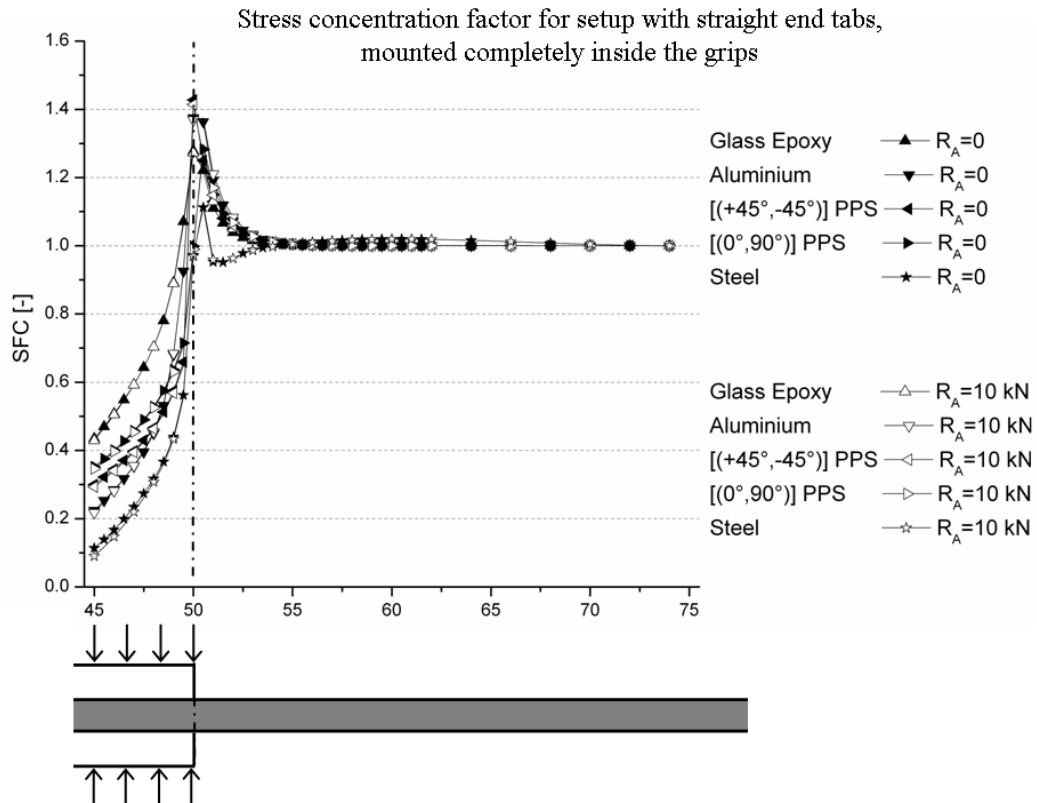


Figure 14 Detail of the evolution of the stress concentration factor along the surface of the specimen for geometry b.

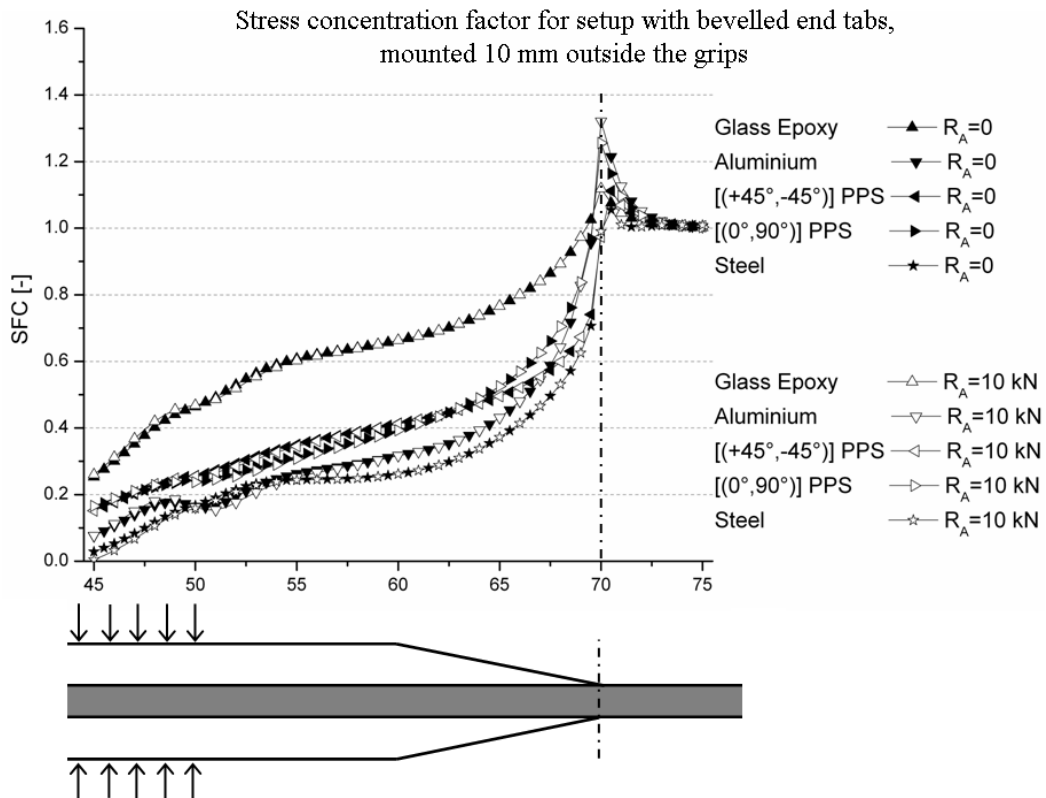


Figure 15 Detail of the evolution of the stress concentration factor along the surface of the specimen for geometry c.

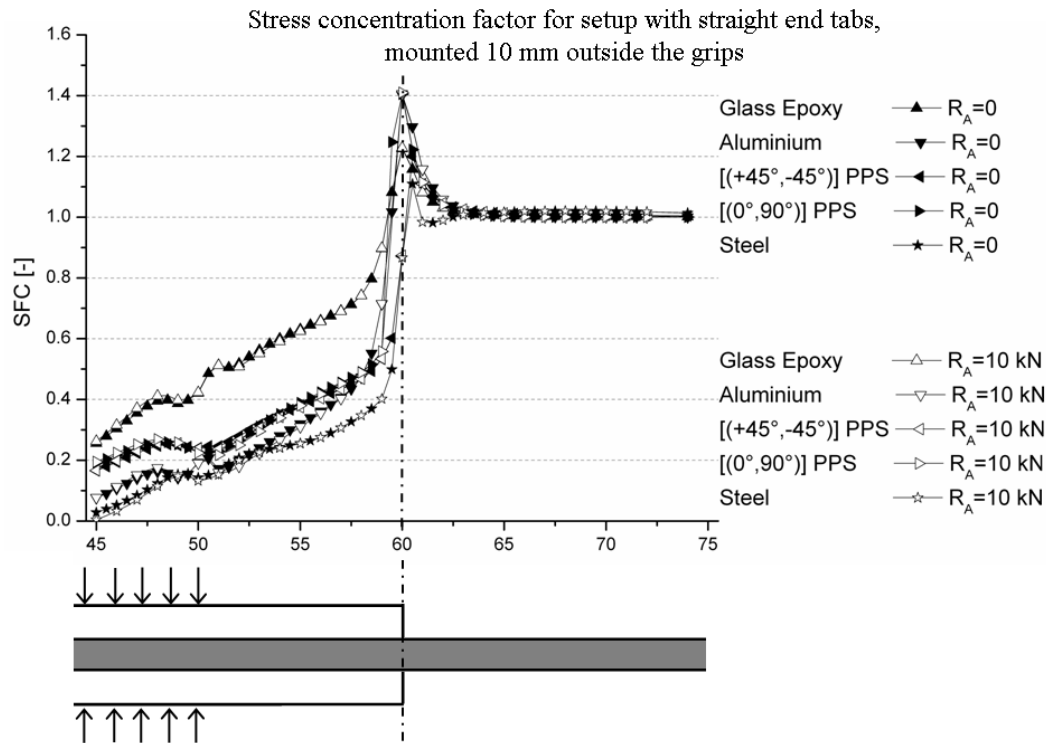


Figure 16 Detail of the evolution of the stress concentration factor along the surface of the specimen for geometry d.

Table 6 Stress concentration factors for the mechanical clamps ( $R_A = 0$  N).

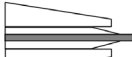
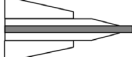
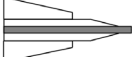
$R_A = 0$ N	Glass-epoxy	Aluminium	C-PPS [(45°, -45°)]	C-PPS [(0°, 90°)]	Isotropic
	1.12	1.32	1.12	1.26	1.05
	1.28	1.37	1.43	1.28	1.11
	1.12	1.32	1.11	1.26	1.06
	1.23	1.40	1.20	1.41	1.11

Table 7 Stress concentration factors for the hydraulic clamps ( $R_A = 10$  kN).

$R_A = 10$ kN	Glass-epoxy	Aluminium	C-PPS [(45°, -45°)]	C-PPS [(0°, 90°)]	Isotropic
	1.12	1.32	1.12	1.26	1.05
	1.27	1.37	1.41	1.30	1.12
	1.12	1.32	1.11	1.26	1.06
	1.23	1.41	1.20	1.41	1.11

As could be expected, the stress concentration factors are the lowest for the isotropic material. It can also be seen that the contact pressure has very limited effect on these factors. In general, it may also be concluded that the bevelled tabs have lower stress concentration factors than the straight end tabs. From these tables, it can be concluded

that the best setup for the presented material is to use either chamfered glass fabric reinforced epoxy or carbon fabric reinforced PPS tabs with the  $[(45^\circ, -45^\circ)]_{4s}$  lay-up.

Of course, what is mentioned above is only theoretical. An important remark must be made about the bonding of the tabs on the specimen. It is well known that thermoplastics do not bond easily and because of the chemical inertness of the polyphenylene sulphide, the latter surely is no exception. After numerous tests with different types of adhesives, the authors have come to the conclusion that, from all the combinations mentioned, PPS is bonded best to PPS. And even in this case, problems occur. Figure 17 illustrates the failure of the bond between the tabs and the specimen. In order to visualise this, both specimen and tabs were first painted white and afterwards, horizontal lines were drawn. This bond-failure already occurs at stresses lower than a third of the ultimate stress. In this figure, it is illustrated for setup with straight end tabs, mounted outside the grips, but it also occurs for the other three setups.

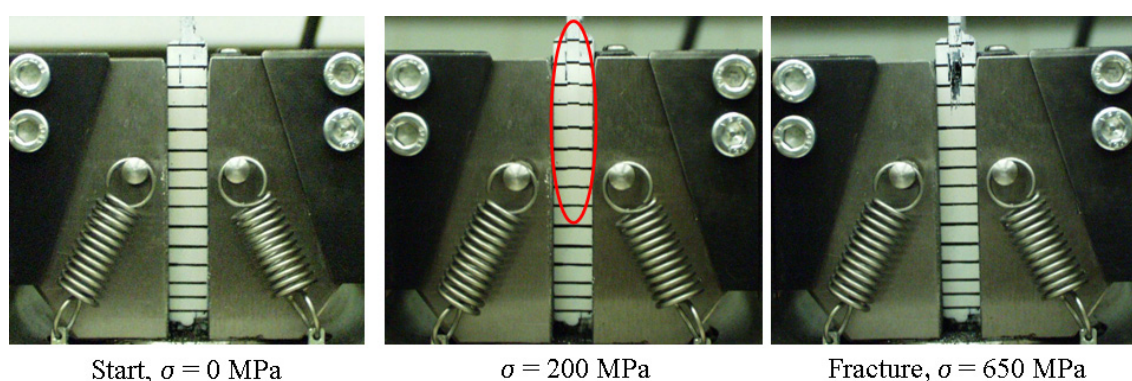


Figure 17 Illustration of the breaking of the bond between the tabs and the specimen, resulting in tab failure.

When performing a quasi-static test, sometimes the fracture occurs outside the tabs, but in a fatigue test, the breaking of the bond has a second effect. Since tab and specimen are no longer attached, the specimen is able to move inside the tabs. Because of the contact pressure applied by the grips, friction occurs, resulting in both wear and heating of the specimen. Since softening of the PPS already occurs at 90 °C, it is no exception that the specimen breaks inside the tabs after very few cycles, not because fatigue life is reached, but because of the friction.

Another consequence of the lack of bonding is that theoretically, setups a, c and d become setup b once the bond is broken over a certain length. If this is considered, together with the fact that only PPS is bonded relatively well to PPS, than it may be concluded from both Table 6 and Table 7 that a straight  $[(0^\circ, 90^\circ)]_{4s}$  carbon fabric reinforced PPS tab gives best results. Since even in this case, the bond tends to break over a length of a few cm's, the authors have experimented with short tabs, with a length approximately equal to the width of the specimen. In this case, if the bond does not break within the first cycles, it tends to last the entire fatigue lifetime of the specimen. However, further research will be necessary.

## 5. Conclusions

A finite element model of a tensile clamp was developed to verify the analytical model of the contact pressure. This model proved excellent correspondence between the simulated and the predicted contact pressure.

Based on this conclusion, a simplified finite element model which uses the analytical model was developed to investigate which end tab geometry gives best results for tension tests on a carbon fabric reinforced thermoplastic, namely polyphenylene sulphide. Four different geometries and four different material combinations were examined. From these simulations, it could be concluded that a chamfered glass-epoxy or carbon PPS with a  $[(45^\circ, -45^\circ)]_{ns}$  gave lowest stress concentration factors. However, due to the chemical inertness of the used material, resulting in a poor bond between tab and specimen, the authors propose to use short straight end tabs with a  $[(0^\circ, 90^\circ)]_{4s}$  lay-up and to mount the specimen in such a way that the end tabs are completely between the grips.

### Acknowledgements

The authors are highly indebted to the university research fund BOF (Bijzonder Onderzoeksfonds UGent) for sponsoring this research and to Ten Cate Advanced Composites for supplying the material.

### References

- [1] I. De Baere, W. Van Paepegem, J. Degrieck, H. Sol, D. Van Hemelrijck and A. Petreli, *Comparison of different identification techniques for measurement of quasi-zero Poisson's ratio of fabric reinforced laminates*. Accepted for *Composites part A*
- [2] I. De Baere, W. Van Paepegem, J. Degrieck, *Design of mechanical clamps with extra long wedge grips for static and fatigue testing of composite materials in tension and compression*, accepted for *Experimental Techniques*.
- [3] De Waele W, Degrieck J, De Baets P, Moerman W, Taerwe L, Feasibility of integrated optical fibre sensors for condition monitoring of composite structures - Part II: Combination of Bragg-sensors and acoustic emission detection. *INSIGHT* 45 (8): 542-+ AUG 2003.
- [4] De Waele W, Degrieck J, Baets R, Moerman W, Taerwe L, Load and deformation monitoring of composite pressure vessels by means of optical fibre sensors. *INSIGHT* 43 (8): 518-525 AUG 2001.
- [5] C.S. Shin and C.C. Chiang, Fatigue damage monitoring in polymeric composites using multiple fibre Bragg gratings. *International Journal of Fatigue*, Volume 28, Issue 10, October 2006, Pages 1315-1321, The Third International Conference on Fatigue of Composites.
- [6] Larissa Sorensen, Thomas Gmür and John Botsis, Residual strain development in an AS4/PPS thermoplastic composite measured using fibre Bragg grating sensors, *Composites Part A: Applied Science and Manufacturing* 37 (2) Feb 2006 270-281
- [7] Seo DC, Lee JJ, Damage detection of CFRP laminates using electrical resistance measurement and neural network, *Composite Structures* 47 (1-4): 525-530 DEC, 1999
- [8] Angelidis N, Wei CY, Irving PE, The electrical resistance response of continuous carbon fibre composite laminates to mechanical strain, *Composites Part A –Applied Science and Manufacturing* 35 (10): 1135-1147, 2004
- [9] Park JB, Okabe T, Takeda N, New concept for modelling the electromechanical behaviour of unidirectional carbon-fibre-reinforced plastic under tensile loading, *Smart Materials & Structures* 12 (1): 105-114 FEB, 2003
- [10] Irving PE, Thiagarajan C, Fatigue damage characterization in carbon fibre composite materials using an electrical potential technique, *Smart Materials & Structures* 7 (4): 456-466 AUG, 1998
- [11] De Baere I, Van Paepegem W and Degrieck, J. The use of rivets for electrical resistance measurement on carbon fibre-reinforced thermoplastics, *Submitted to Smart*

De Baere, I., Van Paepegem, W. and Degrieck, J. (2009). On the Design of End Tabs for Quasi-Static and Fatigue Testing of Fibre-Reinforced Composites. *Polymer Composites*, 30(4), 381-390.

*Materials and Structures*